



Accepted Article

Title: Aggregation-Induced Emission Gemini Surfactant-Assisted Fabrication of Shape-Controlled Fluorescent Hollow Mesoporous Silica Nanoparticles

Authors: Saisai Yan, Gao Zhinong, Yan Xia, Xueming Liao, Jia Han, Chenchen Pan, Yingfang Zhang, and Wenzhong Zhai

This manuscript has been accepted after peer review and appears as an Accepted Article online prior to editing, proofing, and formal publication of the final Version of Record (VoR). This work is currently citable by using the Digital Object Identifier (DOI) given below. The VoR will be published online in Early View as soon as possible and may be different to this Accepted Article as a result of editing. Readers should obtain the VoR from the journal website shown below when it is published to ensure accuracy of information. The authors are responsible for the content of this Accepted Article.

To be cited as: *Eur. J. Inorg. Chem.* 10.1002/ejic.201800280

Link to VoR: <http://dx.doi.org/10.1002/ejic.201800280>

Aggregation-Induced Emission Gemini Surfactant-Assisted Fabrication of Shape-Controlled Fluorescent Hollow Mesoporous Silica Nanoparticles

Saisai Yan,^[a, b] Zhinong Gao,^{*[a, b]} Yan Xia,^[a, b] Xueming Liao,^[a, b] Jia Han,^[a, b] Chenchen Pan,^[a, b] Yingfang Zhang^[a, b] and Wenzhong Zhai^[a, b]

Abstract: Development of particles that possess different properties has been a long-thought goal for producing multifunctional materials due to their combination of performance. Herein, aggregation-induced emission (AIE) gemini surfactant-assisted preparation of shape-controlled fluorescent hollow silica nanoparticles (AIE-SNs) is performed directly in water via a one-pot method. The incorporated AIE gemini surfactant (C₁₆-TPE-C₁₆) will not only provide fluorophore for AIE-SNs but also participate in the structure-directing process with cetyltrimethylammonium bromide (CTAB) to regulate their construction. By properly tuning the molar ratio of CTAB and C₁₆-TPE-C₁₆, AIE-SNs with different morphologies and fluorescence can be produced directly. Their derived mesoporous silica nanoparticles (AIE-MSNs) can also be well fabricated by subsequent extraction owing to the inherent structural differences of CTAB and C₁₆-TPE-C₁₆. Importantly, fluorescent hollow mesoporous silica nanorods and nanospheres with ordered channels, thin shell thickness (~13 and ~7 nm), high accessible surface area (599.2 and 573.9 m²/g) and uniform pore size (~2.8 nm) can be facily prepared when the molar ratio of CTAB and C₁₆-TPE-C₁₆ was determined at 30:1 and 15:1, respectively. This facile and straightforward method for creating tunable hollow AIE-MSNs may open viable opportunities and inspiration for the preparation of particles with multiple properties.

Introduction

Silica nanoparticles (SNs) have been intensively pursued over the past few decades due to their fascinating features and properties including ideal chemical stability, rigid structure, uniform and tunable pore structure, facile surface functionalization and good biocompatibility.^[1] Silica has received "generally recognized as safe" status designated by U.S. Food and Drug Administration (FDA), as demonstrated by its common usage in the food additives and vitamin supplements.^[2] In particular, mesoporous silica nanoparticles (MSNs) have been widely employed as promising candidate carriers for drug delivery and building blocks for stimuli-responsive systems.^[3] It has been reported that numerous functional materials such as magnetic nanoparticles, dyes, proteins and anticancer drugs could be incorporated into MSNs, thus protecting them from the

adverse environments and enhancing their performance in living organisms.^[4] Moreover, MSNs allow for straightforward, diffusion-controlled cargo entrapment and can be functionalized to release the loaded drug in response to chosen stimuli.^[5] With the development of synthetic nanoscience and nanotechnology, the advanced hollow MSNs have been gradually fabricated by various methods.^[6] Hollow MSNs can provide both large cavities and mesoporous shells compared with conventional MSNs, affording high storage/adsorption capacity and accessible channels for mass transfer and diffusion.^[7] Similarly, sustained-release behavior and synergistic effects of loaded materials can also be realized with the help of hollow MSNs, showing great potential in biomedical applications.^[8]

In recent years, nanochemistry research has moved toward the realization of complex multifunctional nanoplatform, which able to combine two or more different features into a single nanosystem by a synergic way. These integrated nanosystems provide new degrees of freedom to control nanoparticles functionality.^[1c, 2b] In this context, the combination of hollow mesoporous and fluorescence into one nanostructure has attracted great interest due to their enormous potential in construction of complex nanoplatform and ultimately multifunctional materials.^[9] Different from conventional fluorescent dyes, aggregation-reduced emission (AIE) molecules with the opposite characteristics to the aggregation-caused quenching (ACQ) are an important and novel category of fluorogens that emit more efficiently while in aggregated state than in dispersed state.^[2b, 10] Since Tang and his team members reported on the AIE compounds in 2001,^[11] the development of AIE molecules has opened new opportunities for biological sensing and imaging applications, and a great many of AIE-based materials have been designed and investigated.^[12] Even so, their performances are severely limited by the poor water solubility in practical application. Considering the fluorescent mechanism of AIE molecules, it is possible to obtain fluorescent nanomaterials with stronger photobleaching resistance by taking advantage of the rigid structures provided by silica matrix to restrict the intramolecular rotations of AIE molecules.^[2a] Recently, novel multi-stable fluorescent SNs have been prepared from in situ doping with AIE molecules.^[1b] The AIE molecules can be stabilized in the rigid microenvironment provided by SNs and thereby achieve environmental tolerance. Additionally, the covalent binding AIE-SNs, rather than physically blended, have also been developed in order to avoid the AIE molecules leak out from the SNs.^[7, 13] However, the preparations of those MSNs-based fluorescent hollow nanosystems are always complicated and accompanied by troublesome procedures. Meanwhile, their morphologies can only be determined by the confined silica during the modification. Continuous efforts to investigate nano-bio interactions have revealed that nanoparticles with elongated

[a] Dr. S. Yan, Prof. Dr. Z. Gao*, Dr. Y. Xia, Dr. X. Liao, J. Han, C. Pan, Y. Zhang, Dr. W. Zhai
College of Chemistry and Molecular Sciences,
Wuhan University, Wuhan 430072, P.R. China.
E-mail: gzn@whu.edu.cn

[b] Key Laboratory of Biomedical Polymers,
Ministry of Education of China,
Wuhan 430072, Hubei, P.R. China.

Supporting information for this article is given via a link at the end of the document

shapes have advantages over spherical nanoparticles.^[14] It is urgent to overcome the shape limitation and pursue facile and straightforward approach to meet different applications.

Gemini surfactants represent a new class of surfactants and contain one unique structure of two amphiphilic moieties connected with a spacer. They usually have better interfacial properties, such as lower critical micelle concentrations (CMC), miscellaneous aggregate morphologies, greater solubilization and enhanced surface activities, than the corresponding single-chain surfactants.^[15] Our group has been mainly focused on the research of gemini surfactant with novel structures and properties, as well as their application in templated preparation of nanoparticles.^[16] Their strong aggregation ability and charged head groups make them an ideal template agent for the preparation of various nanostructures.

In this work, we firstly design and synthesize a unique cationic fluorescent gemini surfactant (denoted as C_{16} -TPE- C_{16}) containing the typical tetraphenylethene (TPE) luminophore and hexadecyl group. Subsequently, tunable AIE-SNs were prepared directly in water via a one-pot method under the cooperative structure direction of cetyltrimethylammonium bromide (CTAB) and C_{16} -TPE- C_{16} (Scheme 1). The incorporated C_{16} -TPE- C_{16} will not only provide fluorophore for AIE-SNs but also cooperate with CTAB to regulate their construction as structure-directing agent. By properly balancing the structure-directing effects of CTAB and C_{16} -TPE- C_{16} , it was possible to control the morphology of AIE-SNs systematically. Finally, their derived AIE-MSNs were fabricated by the HCl/ethanol extraction due to the inherent structural differences of CTAB and C_{16} -TPE- C_{16} . It is worth noting that regular hollow AIE-SNs-30 and AIE-SNs-15 as well as their corresponding AIE-MSNs-30 and AIE-MSNs-15 can be facilely prepared when the molar ratio of CTAB and C_{16} -TPE- C_{16} was determined at 30:1 and 15:1, respectively. To the best of our knowledge, this is the first report on the direct synthesis of shape-controlled fluorescent hollow silica nanoparticles in water, and makes the best use of the intrinsic merits of CTAB and C_{16} -TPE- C_{16} to efficiently prepare their corresponding AIE-MSNs.

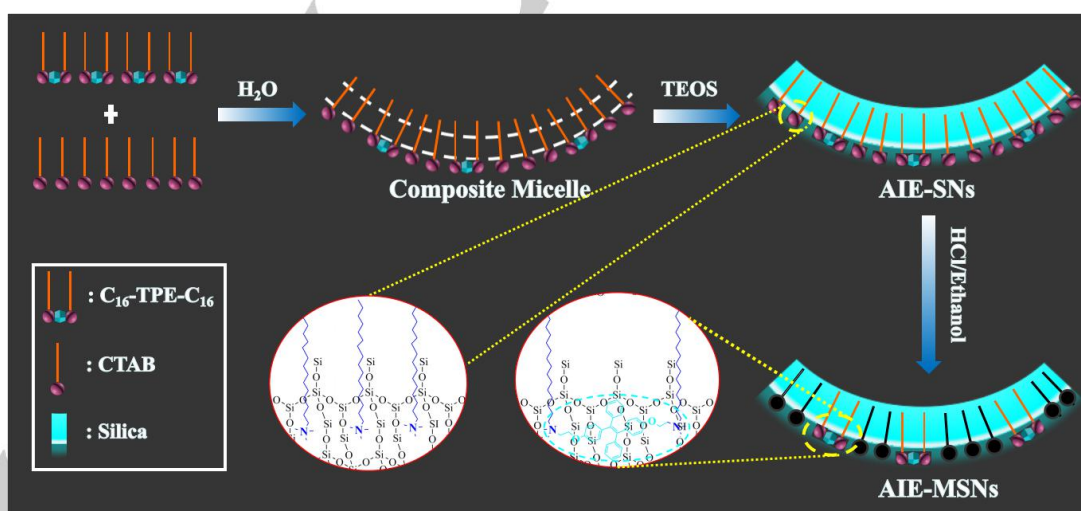
Results and Discussion

Characterization of the C_{16} -TPE- C_{16}

In order to elucidate the structural information of the synthesized compounds in detail, extensive spectral studies like NMR, IR, MS-ESI and UV-Vis absorption spectra were recorded. As shown in Figure S1, the proton signals of TPE (cyan-sign) and intermediate carbon chains (green-sign) can be clearly identified in the ^1H NMR spectra of C_{16} -TPE- C_{16} . It is worth noting that the amphiphilic moieties of C_{16} -TPE- C_{16} possess the same hydrophobic chain length as CTAB. In comparison with CTAB, the other peaks of C_{16} -TPE- C_{16} were corresponded nicely to the alkyl protons of CTAB. In addition, the IR spectra of C_{16} -TPE- C_{16} (Figure S2) exhibited strong characteristic signals at 702, 1509, 1605 and 3019 cm^{-1} corresponding to the stretching vibration of TPE.^[17] The characteristic peak which assigned to $\nu(\text{C-O})$ was also observed at 1241 cm^{-1} . These characteristic peaks suggested the desired chemical structure of C_{16} -TPE- C_{16} .

The surface activity of C_{16} -TPE- C_{16} in aqueous solution was evaluated through the measurement of surface tension, which can be employed to evaluate the CMC. A plot of surface tension (γ) versus the different concentration ($\log C$) of C_{16} -TPE- C_{16} is shown in Figure 1a. Initially, the surfactant unimers were preferentially adsorbed at the air-water interface at low concentrations, thus leading to a constant decrease of the surface tension. With the concentration of C_{16} -TPE- C_{16} continued to increase, the adsorption of surfactant at the air-water interface reached a saturation state and the relative surface tension also came to a balance state after the break point, indicating the formation of micelles.^[18] The CMC of C_{16} -TPE- C_{16} determined from the inflection point in the surface tension curve is 37 μM , which is much lower than that of CTAB (880 μM).^[19]

The CMC value of C_{16} -TPE- C_{16} could also be measured readily by electrical conductivity method. The conductivity (κ) of



Scheme 1. Schematic illustration of the main procedures in the formation process of AIE-MSNs.

C_{16} -TPE- C_{16} is plotted against different concentrations (C) as shown in Figure 1b. The solution conductivity increased linearly with a higher slope at the low concentration. This straight line was observed with a decreased slope when the concentrations of C_{16} -TPE- C_{16} were above 38 μM , which ascribed to the fact that the ionic micelles have less charge per unit mass than their unimers.^[20] The breakpoint at 38 μM is generally considered to be the CMC of C_{16} -TPE- C_{16} . The resulting CMC value by electrical conductivity method matched well with that obtained from the surface tension measurement.

The optical properties of C_{16} -TPE- C_{16} were investigated by the UV-Vis absorption and fluorescence spectroscopy. As shown in Figure 1c, two characteristic peaks appeared at about 250 and 315 nm in the absorption spectra, which assigned to the absorption of the phenyl groups and the conjugated TPE. Their intensity increased linearly with the concentration of C_{16} -TPE- C_{16} in the range from 0 to 150 μM (Figure S3). Meanwhile, the peak position at 315 nm remained unchanged as the concentration increased. In contrast, a clear peak shift can be observed in the reported aggregates of TPE derivatives.^[21] This difference between C_{16} -TPE- C_{16} and other AIE molecules with a TPE core indicated that the conformation of C_{16} -TPE- C_{16} molecules did not depend on the micelle aggregates.^[18]

The fluorescence emission wavelength of C_{16} -TPE- C_{16} remained at 480 nm (typical TPE pattern of light) as the concentration increased (Figure S4a). As shown in Figure 1d, the fluorescence intensity of the surfactant solution at 480 nm was plotted versus the corresponding concentration of C_{16} -TPE- C_{16} . Two straight lines with different slopes can be found with an inflection point at 36 μM , indicating the change of the aggregation state of C_{16} -TPE- C_{16} .^[22] In addition, the UV-Vis absorption and excitation spectra of C_{16} -TPE- C_{16} in aqueous solutions were recorded below and above CMC (Figure S5). The absorbance is simply proportional to photoluminescence species. The decrease in the slope after the inflection point may be ascribed to the combined effects, including AIE effect, inner filter effect and some other uncertain effects.^[23] The TPE units possibly get more freedom in the non-polar interior of the micelles as compared to the aqueous environment. Inner filter effect could happen if the absorbing molecules are at high concentration, causing the disproportional increasing of photoluminescence intensity with the concentration. The intensity of the excitation light is not constant through the solution and only a small percentage of the excitation light reaches the TPE that are visible for the detection system.^[24] The resulting CMC value by fluorescence measurement matched well with those obtained from the surface tension and conductivity measurement, suggesting that the synthesized C_{16} -TPE- C_{16} was a kind of cationic fluorescent surfactant.

On the other hand, a strong emission can be observed directly from the aqueous solution of C_{16} -TPE- C_{16} . As shown in Figure 1e, the light-up fluorescence of C_{16} -TPE- C_{16} in aqueous solution can be directly observed by naked eye with the assistance of UV lamp (365 nm). The photoluminescence increased for the concentrations ranging from 0 to 150 μM and strong cyan emission can be presented for the high concentration solution.

Such visible fluorescence signals are typical characteristics of AIE surfactant in water without the aid from any organic solvent.^[18, 23] The fluorescence spectrum of C_{16} -TPE- C_{16} in $\text{H}_2\text{O}/\text{THF}$ mixture (50 μM) with different THF fractions (vol, 0-80%) was also investigated (Figure S4b). Compared with other types of TPE derivatives, the photoluminescence decreased as the THF fraction increased from 0 to 80%. Regarding the fluorescence wavelength (λ_{max}), C_{16} -TPE- C_{16} in $\text{H}_2\text{O}/\text{THF}$ solution exhibited progressively red-shifting emission when the THF fraction increased.

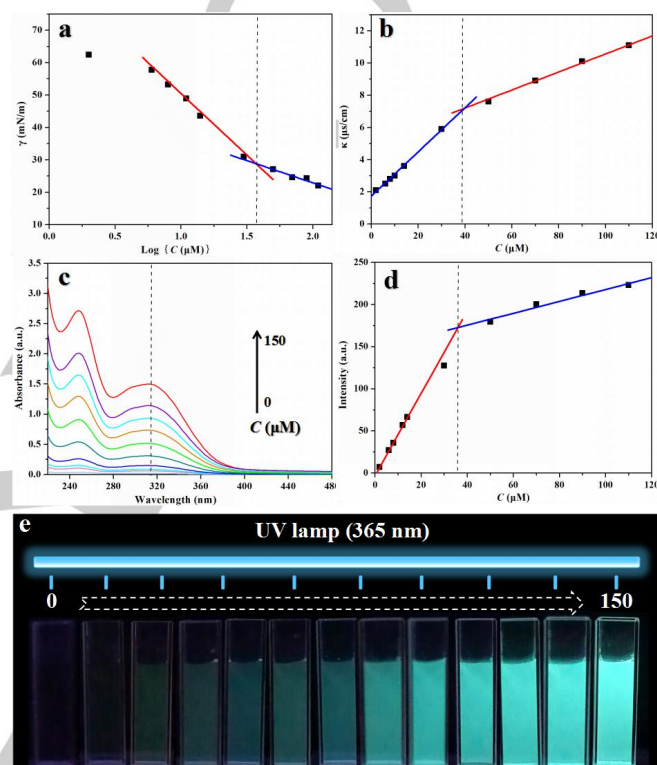


Figure 1. (a) Plot of surface tension (γ) versus \log (concentration) for C_{16} -TPE- C_{16} . (b) Plot of conductivity (κ) versus the concentration of C_{16} -TPE- C_{16} . (c) Absorption spectra of C_{16} -TPE- C_{16} at different concentrations. (d) Plot of fluorescence intensity at 480 nm versus the corresponding concentration of C_{16} -TPE- C_{16} , $\lambda_{\text{ex}} = 325$ nm. (e) Photographs of C_{16} -TPE- C_{16} in aqueous solution at the concentrations from 0 to 150 μM with UV irradiation (365 nm) from the top.

Shape-control of the AIE-SNs and their derived AIE-MSNs

The AIE-SNs in controllable size and shape were prepared via a one-pot method under the cooperative structure direction of CTAB and C_{16} -TPE- C_{16} . As shown in Scheme 1, C_{16} -TPE- C_{16} and CTAB were first dispersed in water to form the composite micelles for the facile island nucleation and growth of silica. When the organosilane precursor (TEOS) was introduced, the hydrolyzed silicate source can be directed to condense around the micellar templates formed by cationic surfactants into ordered silica structures owing to their strong electrostatic interaction.^[3b, 25] Then, a layer of AIE-SNs formed on the composite micelles via the co-assembly of CTAB, C_{16} -TPE- C_{16} and silicate oligomers driven by the electrostatic interaction,

following by the continuing growth and aggregation until the reaction finished. A summary of experimental data and processing parameters are given in Figure S6 and Table S1. The size and shape of AIE-SNs transformed significantly as the molar ratio of CTAB and C₁₆-TPE-C₁₆ changed from 50:1 to 5:1. SEM images are used to characterize the products collected under the different molar ratio of CTAB and C₁₆-TPE-C₁₆ in order to further understand the evolution process of AIE-SNs.

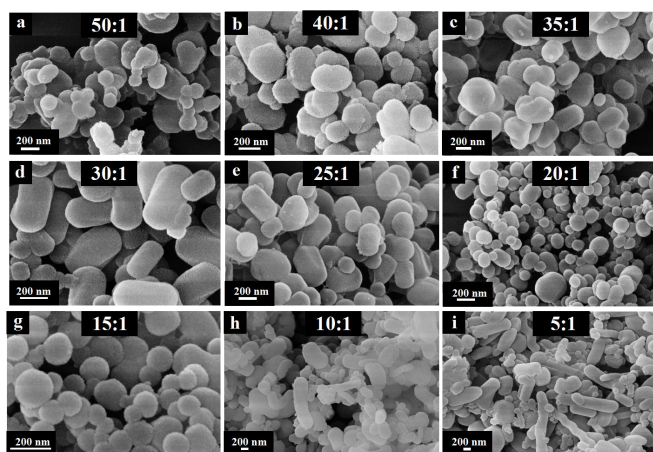


Figure 2. SEM images of AIE-SNs obtained from different molar ratio of CTAB and C₁₆-TPE-C₁₆: (a) 50:1, (b) 40:1, (c) 35:1, (d) 30:1, (e) 25:1, (f) 20:1, (g) 15:1, (h) 10:1 and (i) 5:1.

At the molar ratio of 50:1, the obtained AIE-SNs were mainly large aggregates and small amount of nanospheres (Figure 2a). By judiciously adjusting the molar ratio to 40:1, as expected, the amount of large aggregates became few and the morphology of AIE-SNs gradually evolved into regular shape (Figure 2b). At a fixed molar ratio of 35:1, a variety of product including nanospheres, short nanorods and other irregular nanoparticles can be found (Figure 2c). Remarkably, when the molar ratio was fixed at 30:1, both large aggregates and irregularly shaped nanoparticles disappeared, and the major product evolved into uniform silica nanorods (Figure 2d). Continue decrease the molar ratio of CTAB and C₁₆-TPE-C₁₆ to 25:1, the morphology of AIE-SNs returned to irregular shape and only small amount of silica nanorods can be observed (Figure 2e). At the molar ratio of 20:1, the length of AIE-SNs got truncated to form short nanorods while the main product evolved into nanospheres with small size, thus resulting in a mixture of silica nanospheres and nanorods (Figure 2f). Following this, the short nanorods disappeared and large amount of nanospheres were displayed in the product when the molar ratio was fixed at 15:1 (Figure 2g). By continuously decreasing the molar ratio to 10:1, significant differences were observed and the morphology of formed AIE-SNs returned to irregular shape again (Figure 2h). Interestingly, some of the AIE-SNs tend to cluster into long worm-like morphology and some can even reach to the length of micron in the product. When the ratio was fixed at 5:1, more AIE-SNs showed the elongated rod-like morphology instead of the rounded one in the product (Figure 2i).

It is worth noting that regular hollow AIE-SNs-30 and AIE-SNs-15 can be facily prepared when the molar ratio of CTAB and C₁₆-TPE-C₁₆ was determined at 30:1 and 15:1, respectively. As shown in Figure 3a, the SEM image of AIE-SNs-30 shows their rod-like morphology with the width of ~250 nm and length of ~450 nm. Close observation of the nanorods reveals their relative coarse surface with some tiny cracks (Figure 3b). Additionally, we can clearly see their internal cavity and the shell fragment of damaged AIE-SNs-30 obtained under intense ultrasonic from the high-magnification SEM images (Figure S7). The hollow structure of AIE-SNs-30 can also be confirmed from the TEM images. As shown in Figure 3c, the internal cavities with thin shells are consistent with their external shape. The shell thickness of AIE-SNs-30 is estimated to be ~13 nm (Figure 3d, S8). In contrast, the SEM image of AIE-SNs-15 exhibits their spherical morphology with smaller diameter of ~130 nm (Figure 3e). At a higher magnification, it reveals the rough surface and internal cavity (yellow-sign) of the damaged AIE-SNs-15 (Figure 3f). As can be observed from the TEM image (Figure 3g), the hollow structures of AIE-SNs-15 can be further verified from their rounded internal cavities with thin shell. In comparison with AIE-SNs-30, the shell of AIE-SNs-15 is much thinner with a thickness of only ~7 nm (Figure 3h, S8).

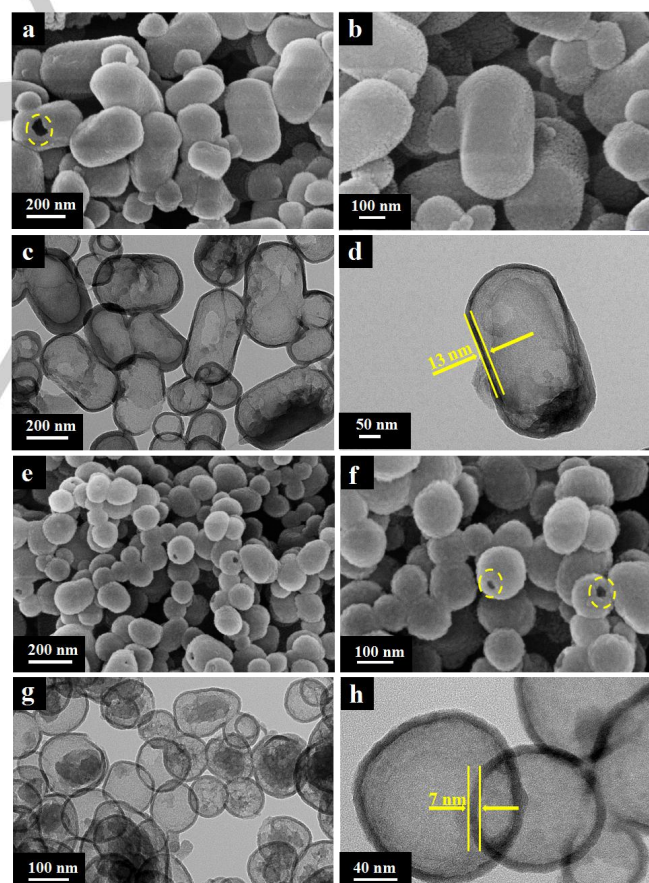


Figure 3. Representative SEM images (a, b) and TEM images (c, d) of AIE-SNs-30. SEM images (e, f) and TEM images (g, h) of AIE-SNs-15. The yellow circles highlight the view of the internal cavities.

Despite the great interest raised by the different kinds of AIE-SNs, the above observations allow us to partially conceive the roles of CTAB and C_{16} -TPE- C_{16} in achieving the shape-controlled AIE-SNs. We propose that the dynamic combined structure-directing effects arising from the cooperative CTAB and C_{16} -TPE- C_{16} can be used to understand the structural evolution process. The original structure-directing effects from pure CTAB were disturbed when C_{16} -TPE- C_{16} was added. At the beginning we can get only disordered AIE-SNs due to the weak effect of insufficient C_{16} -TPE- C_{16} . As the concentration of C_{16} -TPE- C_{16} increased, their contribution to the combined structure-directing effects gradually increased. When the molar ratio of CTAB and C_{16} -TPE- C_{16} reached to 30:1, the combined structure-directing effects were just appropriate for the preparation of uniform nanorods. To further increase the concentration of C_{16} -TPE- C_{16} , their structure-directing effect in the whole system were further increased, following by the continue change for the shape of AIE-SNs. Similarly, new appropriate combined structure-directing effect was provided when the molar ratio of CTAB and C_{16} -TPE- C_{16} reached to 15:1. It was the growing effects of C_{16} -TPE- C_{16} in the structure-directing process that lead to the continue evolution of the construction. The structure-directing effect of C_{16} -TPE- C_{16} can also be confirmed from the preparation of comparing CTAB-SNs. Only uniform nanospheres (~220 nm) with rugged surface are found in the absence of C_{16} -TPE- C_{16} (Figure S9). Meanwhile, it is impossible to get the hollow structure of SNs under the guidance of individual CTAB according to reported literature.^[6, 12a, 26] Additionally, the CTAB acted as the main body in guiding the evolution process of AIE-SNs was also indispensable for the whole system. Only large aggregates composed of small nanoparticles can be obtained under the direction of pure C_{16} -TPE- C_{16} (Figure S10). All these results revealed the combined structure-directing effect arising from the cooperative CTAB and C_{16} -TPE- C_{16} in guiding the evolution process of AIE-SNs. On the basis of this dynamic combined structure-directing effect from CTAB and C_{16} -TPE- C_{16} , it was reasonable to assume that other interesting shapes of AIE-SNs may also be detected beyond our research by adjusting the molar ratio.

On refluxing the AIE-SNs in acidic alcohol, the interaction between the cationic surfactant head group and the anionic silica frame was broken, allowing the templating agent to be removed from the mesopores.^[3b, 27] Thus, the AIE-SNs can be transformed into AIE-MSNs smoothly by removing the CTAB template with HCl/ethanol extraction. Compared with the straight chain structure of CTAB (Figure S1), it is more difficult to remove the C_{16} -TPE- C_{16} from SNs due to their complex structure. In particular, the TPE units in the spacer of C_{16} -TPE- C_{16} can be restricted firmly in the rigid structures (Si-O-Si) provided by silica matrix (Scheme 1). Therefore, large amount of C_{16} -TPE- C_{16} can still be encapsulated in SNs after the removal of embedded CTAB, resulting in the fluorescent property of AIE-MSNs.

SEM and TEM images of the AIE-MSNs-30 and AIE-MSNs-15 were performed to have a better insight of the resulting AIE-MSNs. According to the SEM images (Figure 4a, 4b), the AIE-MSNs preserve their morphologies and displayed no significant external difference with AIE-SNs (Figure 3). The same result can

also be observed from the SEM images of CTAB-SNs and CTAB-MSNs (Figure S9). This indicates that their appearance can be well maintained in the extraction process. As can be observed from the TEM images of AIE-MSNs-30 (Figure 4c, S11), the nanorods retain their hollow structures after the extraction process, while their shells turn to indistinct due to the existence of numerous pores. At a higher magnification (Figure 4e, S11), highly ordered mesoporous channels can be clearly observed in the nanorods. Moreover, the shell thickness of AIE-MSNs-30 is estimated to be ~13 nm, showing no obvious change in size compared with AIE-SNs-30. In contrast, the AIE-MSNs-15 also retain their hollow structures and exhibit the indistinct rounded internal cavity (Figure 4d, S11). TEM images of AIE-MSNs-15 at a higher magnification (Figure 4f, S11) further revealed their ordered pore structures and the same shell thickness (~7 nm) as AIE-SNs-15. Despite the additional large numbers of pores on the shells, both the internal cavity and external morphologies were preserved after the CTAB was removed, implying their excellent structural stability.

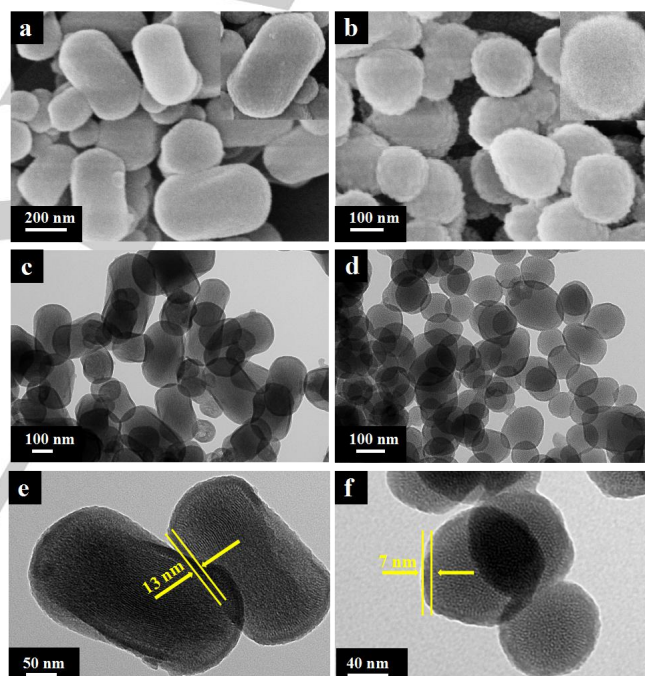


Figure 4. Representative SEM images (a) and TEM images (c, e) of AIE-MSNs-30. SEM images (b) and TEM images (d, f) of AIE-MSNs-15.

Characterization of the AIE-SNs and AIE-MSNs

The SNs can provide a rigid environment composed of Si-O-Si skeletons for AIE molecules.^[1b] In order to confirm the fact that C_{16} -TPE- C_{16} had been encapsulated into SNs successfully, fluorescence and UV-Vis absorption spectroscopy were used to evaluate the obtained AIE-SNs and supernatant solution at the end of the reaction. Fluorescence spectra for different kinds of AIE-SNs with the same concentration of 0.25 mg/mL are shown in Figure 5a. The fluorescence intensity of AIE-SNs was very strong and enhanced with the molar ratio changed from 50:1 to 5:1 compared with CTAB-SNs. As shown in Figure 5b, the UV-Vis absorption of C_{16} -TPE- C_{16} occurred at 315 nm, and one

strong and broad band from 200 to 400 nm appeared for CTAB-SNs correspond to scattering of SNs. Besides the scattering of SNs, AIE-SNs showed apparent absorption at around 328 nm belonging to C_{16} -TPE- C_{16} with a red shift at around 13 nm, which might be attributed to intermolecular energy transfer inside of AIE-SNs.^[1b] At the same time, the UV-Vis absorbance and fluorescent intensity of supernatant solution was measured after the AIE-SNs were removed with centrifugation (Figure S12). Only broad band appeared in the UV-Vis absorption spectrum of the supernatant solution. According to the linear relationship between the optical absorbance data and concentrations of C_{16} -TPE- C_{16} (Figure S3), there almost no remaining C_{16} -TPE- C_{16} in supernatant solution left compared with the initial concentration (Table S1). Their fluorescence intensity was also very weak and the emission wavelength occurred at 467 nm instead of 480 nm (Figure S12b). These results suggested that the C_{16} -TPE- C_{16} have been doped into SNs successfully.

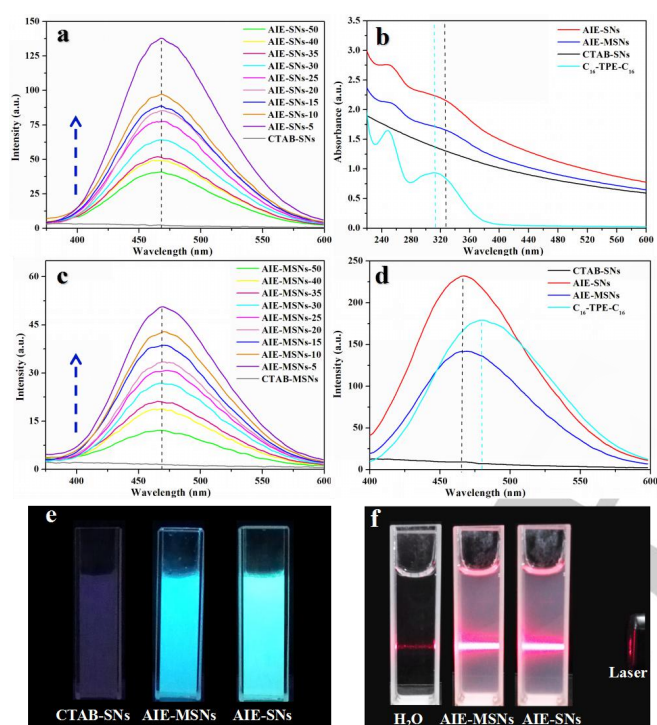


Figure 5. (a) Fluorescence spectra for different kinds of AIE-SNs with the same concentration of 0.25 mg/mL, $\lambda_{\text{ex}} = 325$ nm. (b) Absorption spectra of AIE-SNs, AIE-MSNs, CTAB-SNs and C_{16} -TPE- C_{16} . (c) Fluorescence spectra for different kinds of AIE-MSNs with the same concentration of 0.25 mg/mL, $\lambda_{\text{ex}} = 325$ nm. (d) Fluorescence spectra of CTAB-SNs, AIE-SNs, AIE-MSNs and C_{16} -TPE- C_{16} , $\lambda_{\text{ex}} = 325$ nm. (e) Fluorescent photographs of CTAB-SNs, AIE-SNs and AIE-MSNs in aqueous dispersion taken under UV irradiation (365 nm). (f) Tyndall phenomenon of H_2O , AIE-MSNs and AIE-SNs in aqueous dispersion.

The fluorescence and UV-Vis absorption spectroscopy were also used to evaluate the presence of C_{16} -TPE- C_{16} in AIE-MSNs. The fluorescence spectra for different kinds of AIE-MSNs with the same concentration of 0.25 mg/mL were displayed in Figure 5c. In comparison with CTAB-MSNs, their fluorescence intensity was strong and increased with the species changed from AIE-

MSNs-50 to AIE-MSNs-5. Undesirably, their fluorescent intensity was decreased compared to the same amount of AIE-SNs (Figure 5a), as a consequence of the simultaneous leaching of C_{16} -TPE- C_{16} during the extraction. Even so, the rest can continue to provide fluorescence for the MSNs. The fluorescence spectra of CTAB-SNs, AIE-SNs, AIE-MSNs and C_{16} -TPE- C_{16} are shown in Figure 5d. The emission wavelength (467 nm) of AIE-MSNs occurred as same as AIE-SNs, which reflected the same aggregate state of C_{16} -TPE- C_{16} in SNs before and after removal of the CTAB. Similarly, the UV-Vis absorption of AIE-MSNs also showed the same peak as AIE-SNs at around 328 nm (Figure 5b). On the other hand, as shown in the Figure 5e, bright cyan color can be clearly observed from the presented photographs of both AIE-SNs and AIE-MSNs in aqueous dispersion when they were excited by the UV lamp (365 nm). In contrast, there is no distinct light emitted from the CTAB-SNs. As a kind of inorganic nanoparticles, a typical Tyndall phenomenon has been observed from AIE-SNs and AIE-MSNs (Figure 5f). This result has further confirmed the successful preparation and excellent dispersibility of AIE-SNs and AIE-MSNs.

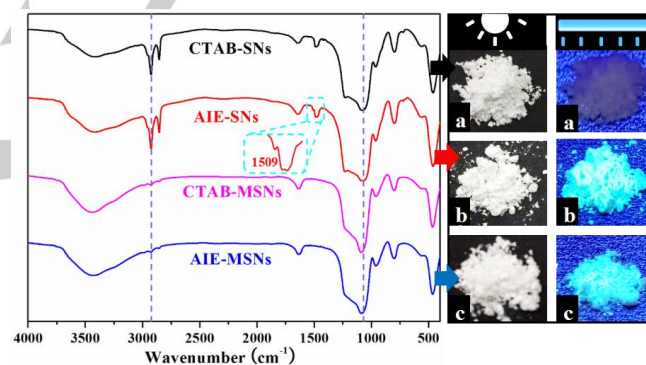


Figure 6. IR spectra of CTAB-SNs (black line), AIE-SNs (red line), CTAB-MSNs (pink line) and AIE-MSNs (blue line). Photographs of the solid powder of CTAB-SNs (a), AIE-SNs (b) and AIE-MSNs (c) taken under the room light and UV irradiation (365 nm).

The IR spectra of CTAB-SNs, AIE-SNs, CTAB-MSNs and AIE-MSNs are given in Figure 6. The strong peaks located at 1083, 961 and 796 cm^{-1} were observed in all of them corresponding to the asymmetric and symmetric stretching vibrations of Si-O-Si.^[12a] Although the amount of C_{16} -TPE- C_{16} is much lower than CTAB in AIE-SNs, its characteristic signal located at 1509 cm^{-1} assigned to the stretching vibration of TPE can still be observed compared to CTAB-SNs. As compared with CTAB-SNs and AIE-SNs, the stretching vibration bands of C-H which located at 2925 and 2857 cm^{-1} were both disappeared in the sample of CTAB-MSNs and AIE-MSNs, suggesting that the CTAB have been removed from SNs successfully by the extraction process.^[12a] It was the smooth departure of CTAB that lead to the formation of large amount of new pores observed in the TEM images of AIE-MSNs (Figure 4, S11). As for the aggregate state, the solid powder of CTAB-SNs, AIE-SNs and AIE-MSNs were both white color in appearance under normal room lighting, but strong cyan light can be emitted from AIE-SNs and AIE-MSNs under UV irradiation of 365 nm (Figure 6a-6c). These results also

suggested that the C₁₆-TPE-C₁₆ molecules have been doped into AIE-SNs and AIE-MSNs successfully.

Change of porosity between AIE-SNs and AIE-MSNs

To better understand the structural properties of AIE-SNs and AIE-MSNs, nitrogen adsorption measurements of AIE-SNs-30, AIE-MSNs-30, AIE-SNs-15 and AIE-MSNs-15 were carried out to investigate their porosity. The resulting adsorption-desorption isotherms and pore size distribution curves are shown in Figure 7. It was found that all the samples exhibited the combination of type II and IV isotherms with a H4 type hysteresis loop, which was nearly parallel over an appreciable range of relative pressure according to the IUPAC classification.^[28] The open H4 type hysteresis loop can be attributed to the mesoporous structures formed by slit-like pores, the aggregation of nanoparticles and internal voids in the AIE-SNs. The nitrogen sorption plot of AIE-SNs-30 displayed a sharp increase of P/P₀ from 0.8 to 1.0, revealing a characteristic mesoporous structure. The BET surface area and pore volume of AIE-SNs-30 were calculated to be 273.3 m²/g and 0.27 cm³/g, respectively. Additionally, the AIE-SNs-30 showed a relatively narrow pore size distribution from 2-3 nm (Figure 7b). Comparatively, the desorption branch of AIE-SNs-15 also exhibited a steep capillary evaporation step at P/P₀ of ~0.8, indicating the existence of mesoporous structure. However, their BET surface area and total pore volume were calculated to be only 56.3 m²/g and 0.12 cm³/g, respectively, which were much lower than those of AIE-SNs-30. The nitrogen adsorption measurements suggested that AIE-SNs-30 have already possessed the available loading-capacity owing to the pores and higher specific surface areas.

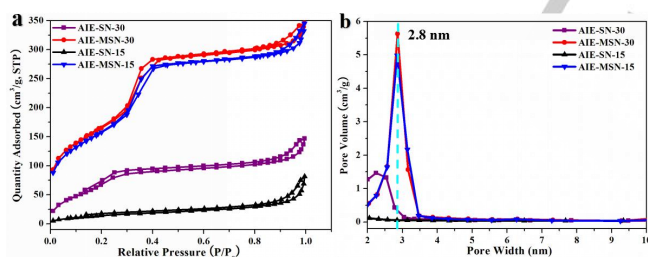


Figure 7. Nitrogen adsorption-desorption isotherms (a) and their corresponding pore size distribution curves (b) of AIE-SNs-30, AIE-MSNs-30, AIE-SNs-15 and AIE-MSNs-15.

As shown in Figure 7a, AIE-MSNs-30 and AIE-MSNs-15 displayed the similar nitrogen sorption isotherms although their initial statuses were significantly different. As a result of the nitrogen adsorption measurements, the calculated BET surface area of AIE-SNs-30 and AIE-SNs-15 increased to 599.2 and 573.9 m²/g, respectively, which were comparable value with many other hollow MSNs reported in literature.^[7, 9, 29] Their corresponding pore volume of AIE-SNs-30 and AIE-SNs-15 were calculated to be 0.60 and 0.59 cm³/g, respectively. Meanwhile, their similar pore size distribution curves of AIE-MSNs-30 and AIE-MSNs-15 in the range of 2-3.5 nm suggested their same mesoporous structure (Figure 7b). The detailed specific surface area and pore volume of these samples were in the order of AIE-MSNs-30 > AIE-MSNs-15 > AIE-SNs-30 > AIE-

SNs-15 (Table S2). The greatly increased surface area and pore volume of AIE-MSNs demonstrated their higher porosity. This result was also consistent with the changed porous structure observed in the TEM images of AIE-SNs and AIE-MSNs (Figure 3, 4). The CTAB template can be removed easily and bring about large amount of new pores when AIE-SNs were treated by extraction. The high specific surface area of AIE-MSNs may facilitate good accessibility of the active material to the surface and contribute to the enhanced loading capacity and delivery performance, while the porous structure allows for rapid and shorter diffusion paths for loading image or therapy agents.

Conclusions

In summary, a one-pot method is developed to prepare tunable hollow AIE-SNs directly in water under the cooperative structure direction of CTAB and C₁₆-TPE-C₁₆. The key feature of this method is that the incorporated C₁₆-TPE-C₁₆ will not only provide fluorophore for AIE-SNs but also participated in the structure-directing process with CTAB to regulate their construction. By properly balancing the structure-directing effects of CTAB and C₁₆-TPE-C₁₆, the morphologies of AIE-SNs can be adjusted from initial large aggregates to nanorods, nanospheres and some other irregular shapes. Furthermore, their derived AIE-MSNs can also be fabricated by subsequent extraction due to the inherent structural differences of CTAB and C₁₆-TPE-C₁₆. Importantly, regular hollow AIE-MSNs-30 and AIE-MSNs-15 with ordered channels, thin shell thickness (~13 and ~7 nm), high accessible surface area (599.2 and 573.9 m²/g) and uniform pore size (~2.8 nm) can be facilely prepared in this process. The present approach based on CTAB and C₁₆-TPE-C₁₆ offered a new convenient way to fabricate particles with multiple properties. Additionally, the proposed hollow AIE-MSNs can provide combined advantages over individual fluorescent, hollow or mesoporous nanoparticles, and have promising potential in biomedical application as multifunctional nanoplatform.

Experimental Section

Materials and instruments.

Zinc dust, 4-hydroxybenzophenone, 1,2-dibromoethane and hexadecyldimethylamine were purchased from Aladdin. TiCl₄, K₂CO₃, Na₂SO₄, CH₂Cl₂, NaOH, ethanol, acetone, pyridine, petroleum ether, hydrochloric acid (HCl), tetrahydrofuran (THF), cetyltrimethylammonium bromide (CTAB) and tetraethylorthosilicate (TEOS) were purchased from Sinopharm Chemical Reagent Co. All reagents were of analytical grade and used without further purification. Water was purified by a Milli-Q system (Millipore, Molsheim, France).

IR spectra were recorded in the range 4000-400 cm⁻¹ using KBr pellets on a Thermo Nicolet 5700 spectrophotometer. ¹H NMR and ¹³C NMR were obtained from a Bruker Ascend-400MHz spectrometer using CDCl₃ or DMSO-*d*₆ as solvent. ESI mass spectra (ESI-MS) were recorded on a LCQ spectrometer (Finnigan, USA). UV-Vis spectra were measured on a Shimadzu UV-2600 spectrophotometer. Fluorescence spectra were

obtained by the RF-5301PC fluorescence spectrometer (Shimadzu) at a slit of 3.0 nm with a fast scanning speed. Dynamic light-scattering (DLS) measurements were measured using a Malvern ZEN3600 Zetasizer (UK) equipped with a 632.8 nm He-Ne laser and an avalanche photodiode detector. The field emission scanning electron microscopy (FE-SEM) images were performed on Zeiss Sigma FESEM (20 KV). Transmission electron microscopy (TEM) images were recorded on a JEM-2100 microscope operated at 200 KV. The surface tension values were measured on a QBZY-2 tensiometer (FANGRUI Corporation, Shanghai, China) following the wilhelmy plate procedure at 25.0 °C. The electrical conductivity was performed on a WTW conductivity meter (inoLab Cond730, Germany) at 25.0 °C. Nitrogen adsorption-desorption isotherms were carried out at 77 K on a Micromeritics ASAP 2020 system (Norcross, USA). The Brunauer-Emmett-Teller (BET) method was utilized to calculate the specific surface areas. The Barrett-Joyner-Halenda (BJH) method was conducted to calculate the sample pore size from the desorption branches of the isotherms.

Preparation of the C₁₆-TPE-C₁₆.

The AIE gemini surfactant C₁₆-TPE-C₁₆ was synthesized according to the procedures described in Scheme S1.

(i) The synthesis of TPE-2OH (compound **1**) was performed by the McMurry reaction as reported previously.^[18, 23] Yield: 46 %. ¹H NMR (400 MHz, CDCl₃): δ 7.11-7.15 (m, 6 H), 7.01-7.10 (m, 4 H), 6.95-7.00 (m, 4 H), 6.54-6.59 (m, 4 H).

(ii) Synthesis of TPE-2Br (compound **2**): TPE-2OH (0.24 g, 0.66 mmol) and K₂CO₃ (0.27 g, 1.98 mmol) were mixed in acetone (30 mL). Then, 1,2-dibromoethane (0.372 g, 1.98 mmol) was added dropwise after stirred for 30 min. The resulting mixture was refluxed for 24 h (monitored by TLC) and cooled down to room temperature. After the filtration of insoluble K₂CO₃, the crude product was obtained by evaporation of solvent. The final product was obtained as a white powder after purification by silica gel chromatography with eluents of petroleum ether/ethyl acetate (8:1 (v/v)). Yield: 75 %. ¹H NMR (400 MHz, DMSO-*d*₆): δ 7.07-7.17 (m, 6 H), 6.93-6.98 (m, 4 H), 6.83-6.89 (m, 4 H), 6.69-6.76 (m, 4 H), 4.21-4.26 (m, 4 H), 3.74-3.79 (m, 4 H). ¹³C NMR (400 MHz, DMSO-*d*₆): 156.81, 144.12, 139.77, 136.60, 132.48, 131.22, 128.23, 126.85, 114.41, 67.99, 32.03.

(iii) Synthesis of C₁₆-TPE-C₁₆: TPE-2Br (0.30 g, 0.52 mmol) and hexadecyldimethylamine (0.42 g, 1.56 mmol) were dissolved in ethyl acetate (20 mL). The resulting mixture was refluxed for 5 days. After the reaction mixture cooled down to room temperature, the white precipitate (crude product) was collected by filtration. The product was further washed with ethyl acetate and recrystallized from ethyl acetate/ethanol at least three times to produce the purified product as a yellowish solid. Yield: 42 %. ¹H NMR (400 MHz, CDCl₃): δ 7.06-7.12 (m, 6 H), 6.96-6.99 (m, 4 H), 6.89-6.93 (m, 4 H), 6.58-6.67 (m, 4 H), 4.37-4.43 (m, 4 H), 4.12-4.16 (m, 4 H), 3.56-3.63 (m, 4 H), 3.45 (s, 12 H), 1.78 (s, 4 H), 1.33 (s, 8 H), 1.23 (s, 44 H), 0.85 (t, 6 H). ¹³C NMR (400 MHz, CDCl₃): 155.42, 143.47, 139.84, 137.73, 132.78, 131.27, 127.81, 126.59, 113.81, 66.31, 62.31, 52.09, 31.94, 29.72, 29.68, 29.64, 29.61, 29.53, 29.49, 29.47, 29.43, 29.39, 29.31, 29.28, 26.28, 22.99, 22.71, 14.18. IR (KBr, cm⁻¹): 3019 (m), 2921 (vs), 2851 (vs), 1605 (s), 1509 (vs), 1467 (s), 1241 (vs), 1177 (s), 1057 (m), 725(m), 702 (s). UV-Vis: λ_{max}=315 nm. MS-ESI (CH₃OH, *m/z*): [M-Br]⁺, calcd 1037.5, found 1037.4; [M-2Br]²⁺/2, calcd 478.8, found 478.6.

Preparation of the AIE-MSNs and CTAB-MSNs .

AIE-MSNs were prepared regularly by two steps with the mixture of CTAB and C₁₆-TPE-C₁₆. Briefly, CTAB and C₁₆-TPE-C₁₆ with a total amount of 0.137 mmol were dissolved in ultrapure water (25 mL) firstly. The molar ratio of CTAB and C₁₆-TPE-C₁₆ was as followed CTAB : C₁₆-TPE-C₁₆ = *n* : 1 (*n* = 50, 40, 35, 30, 25, 20, 15, 10 and 5). Then, the aqueous solution of NaOH (0.180 mL, 2.00 M) was introduced into the solution. The temperature of the mixture was adjusted to 80 °C and kept for 30 min. TEOS (0.50 mL, 2.24 mmol) was added dropwise under vigorous stirring. The mixture was allowed to react for 4 h to give a white precipitate. The obtained product was collected by centrifugation and extensively washed with water and ethanol to yield AIE-SNs. Finally, the synthesized AIE-SNs (0.1 g) were refluxed for 24 h in a solution of ethanol (10.0 mL) and HCl (0.6 mL, 37.4%) to remove the CTAB. The product was collected by centrifugation, washed with water and ethanol extensively and dried in vacuum at 35 °C to yield AIE-MSNs. The preparation of comparing CTAB-MSNs was performed with the same amount of pure CTAB surfactant according to the literature.^[12a]

Acknowledgements

This work was supported by the Fundamental Research Funds for the Chinese Central Universities. (2012203020211).

Keywords: aggregation-induced emission • gemini surfactant • shape-control • fluorescent hollow mesoporous • silica nanoparticles

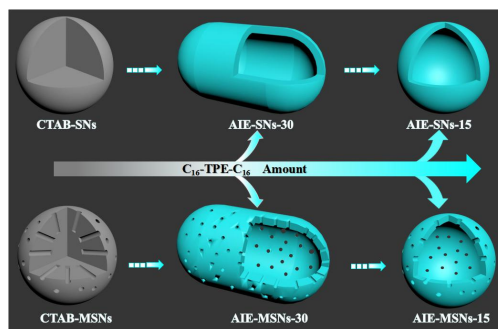
- [1] a) V. Mamaeva, C. Sahlgren, M. Linden, *Advanced drug delivery reviews* **2013**, *65*, 689-702; b) Y.-F. Wang, J. Che, Y.-C. Zheng, Y.-Y. Zhao, F. Chen, S.-B. Jin, N.-Q. Gong, J. Xu, Z.-B. Hu, X.-J. Liang, *Journal of Materials Chemistry B* **2015**, *3*, 8775-8781; c) X. Yao, X. Niu, K. Ma, P. Huang, J. Grothe, S. Kaskel, Y. Zhu, *Small* **2017**, *13*, 1602225-1602235.
- [2] a) D. Li, J. Yu, *Small* **2016**, *12*, 6478-6494; b) L. Yan, Y. Zhang, B. Xu, W. Tian, *Nanoscale* **2016**, *8*, 2471-2487.
- [3] a) S. Mura, J. Nicolas, P. Couvreur, *Nature materials* **2013**, *12*, 991-1003; b) Z. Li, J. C. Barnes, A. Bosoy, J. F. Stoddart, J. I. Zink, *Chemical Society reviews* **2012**, *41*, 2590-2605.
- [4] a) S. Sreejith, X. Ma, Y. Zhao, *Journal of the American Chemical Society* **2012**, *134*, 17346-17349; b) L. He, T. Chen, Y. You, H. Hu, W. Zheng, W. L. Kwong, T. Zou, C. M. Che, *Angewandte Chemie* **2014**, *53*, 12532-12536; c) D. Li, R. Yi, J. Tian, J. Li, B. Yu, J. Qi, *Chemical communications* **2017**, *53*, 8902-8905.
- [5] J. Zhou, N. Hao, T. De Zoyza, M. Yan, O. Ramstrom, *Chemical communications* **2015**, *51*, 9833-9836.
- [6] X. Du, J. He, *Nanoscale* **2011**, *3*, 3984-4002.
- [7] Z. Fan, D. Li, X. Yu, Y. Zhang, Y. Cai, J. Jin, J. Yu, *Chemistry-A European Journal* **2016**, *22*, 3681-3685.
- [8] a) Y. Zhu, J. Shi, W. Shen, X. Dong, J. Feng, M. Ruan, Y. Li, *Angewandte Chemie* **2005**, *117*, 5213-5217; b) T. Wang, F. Chai, Q. Fu, L. Zhang, H. Liu, L. Li, Y. Liao, Z. Su, C. Wang, B. Duan, D. Ren, *Journal of Materials Chemistry* **2011**, *21*, 5299-5306; c) L. Li, F. Tang, H. Liu, T. Liu, N. Hao, D. Chen, X. Teng, J. He, *ACS Nano* **2010**, *4*, 6874-6882.
- [9] Y. Yang, M. Yu, H. Song, Y. Wang, C. Yu, *Nanoscale* **2015**, *7*, 11894-11898.
- [10] J. Mei, Y. Hong, J. W. Lam, A. Qin, Y. Tang, B. Z. Tang, *Advanced materials* **2014**, *26*, 5429-5479.

- [11] J. Luo, Z. Xie, J. W. Y. Lam, L. Cheng, B. Z. Tang, H. Chen, C. Qiu, H. S. Kwok, X. Zhan, Y. Liu, D. Zhu, *Chemical communications* **2001**, 1740-1741.
- [12] a) X. Zhang, X. Zhang, S. Wang, M. Liu, Y. Zhang, L. Tao, Y. Wei, *ACS applied materials & interfaces* **2013**, *5*, 1943-1947; b) R. Hu, N. L. Leung, B. Z. Tang, *Chemical Society reviews* **2014**, *43*, 4494-4562.
- [13] D. Li, Y. Zhang, Z. Fan, J. Yu, *Chemical communications* **2015**, *51*, 13830-13833.
- [14] Z. Wang, Z. Chang, M. Lu, D. Shao, J. Yue, D. Yang, X. Zheng, M. Li, K. He, M. Zhang, L. Chen, W. F. Dong, *Biomaterials* **2018**, *154*, 147-157.
- [15] a) Q. Zhang, Z. Gao, F. Xu, S. Tai, X. Liu, S. Mo, F. Niu, *Langmuir* **2012**, *28*, 11979-11987; b) B. Li, Q. Zhang, Y. Xia, Z. Gao, *Colloids and Surfaces A* **2015**, *470*, 211-217.
- [16] a) Y. Xia, Z. Gao, X. Liao, C. Pan, Y. Zhang, X. Feng, *CrystEngComm* **2017**, *19*, 6547-6555; b) X. Liao, Z. Gao, Y. Xia, F. Niu, W. Zhai, *Langmuir* **2017**, *33*, 3304-3310; c) F. Xu, H. Hou, Z. Gao, *Chemphyschem* **2014**, *15*, 3979-3986.
- [17] Y. Qian, H. Liu, H. Tan, Q. Yang, S. Zhang, L. Han, X. Yi, L. Huo, H. Zhao, Y. Wu, L. Bai, X. Ba, *Macromolecular rapid communications* **2017**, *38*, 1600684-1600690.
- [18] W. Guan, W. Zhou, C. Lu, B. Z. Tang, *Angewandte Chemie* **2015**, *54*, 15160-15164.
- [19] Michael T. Yacilla, Kathleen L. Herrington, a. Laura L. Brasher, E. W. Kaler, S. C. and, J. A. Zasadzinski, *Journal of Physical Chemistry* **1996**, *100*, 5874-5879.
- [20] L. Shi, D. Lundberg, D. G. Musaev, F. M. Menger, *Angewandte Chemie* **2007**, *119*, 5993-5995.
- [21] S.-B. Han, H.-J. Kim, D. Jung, J. Kim, B.-K. Cho, S. Cho, *The Journal of Physical Chemistry C* **2015**, *119*, 16223-16229.
- [22] Y. Xia, L. Dong, Y. Jin, S. Wang, L. Yan, S. Yin, S. Zhou, B. Song, *Journal of Materials Chemistry B* **2015**, *3*, 491-497.
- [23] W. Guan, S. Wang, C. Lu, B. Z. Tang, *Nature communications* **2016**, *7*, 11811-11817.
- [24] B. Valeur, *Molecular Fluorescence: Principles and Applications*, Wiley-VCH, **2001**.
- [25] a) S. H. Wu, Y. Hung, C. Y. Mou, *Chemical communications* **2011**, *47*, 9972-9985; b) K. Suzuki, K. Ikari, H. Imai, *Journal of the American Chemical Society* **2004**, *126*, 462-463.
- [26] A. Taguchi, F. Schüth, *Microporous and Mesoporous Materials* **2005**, *77*, 1-45.
- [27] K. K. Coti, M. E. Belowich, M. Liong, M. W. Ambrogio, Y. A. Lau, H. A. Khatib, J. I. Zink, N. M. Khashab, J. F. Stoddart, *Nanoscale* **2009**, *1*, 16-39.
- [28] K. S. W. Sing, *Pure & Applied Chemistry* **1985**, *57*, 603-619.
- [29] Y. Q. Yeh, B. C. Chen, H. P. Lin, C. Y. Tang, *Langmuir* **2006**, *22*, 6-9.

Entry for the Table of Contents

FULL PAPER

C_{16} -TPE- C_{16} assisted fabrication of shape-controlled hollow AIE-SNs and AIE-MSNs was performed facilely via a straightforward procedure. By properly balancing the structure-directing effects of CTAB and C_{16} -TPE- C_{16} , the morphologies of AIE-SNs and AIE-MSNs can be adjusted from initial non-fluorescent CTAB-SNs to fluorescent nanorods, nanospheres and some other irregular shapes.



Saisai Yan, Zhinong Gao,* Yan Xia, Xueming Liao, Jia Han, Chenchen Pan, Yingfang Zhang and Wenzhong Zhai

Page No. – Page No.

Aggregation-Induced Emission Gemini Surfactant-Assisted Fabrication of Shape-Controlled Fluorescent Hollow Mesoporous Silica Nanoparticles